Geophysical Research Letters

RESEARCH LETTER
10.1029/2018GL079954

Key Points:
- Floodwater impact on Galveston Bay optical-geochemical properties was observed even 1 month following Hurricane Harvey
- Ocean color algorithms applied to VIIRS imagery revealed spatiotemporal response of dissolved and particulate matter following Harvey
- Organic carbon exported from Galveston Bay to shelf waters during/following Hurricane Harvey was comparable to that of a large river

Supporting Information:
- Supporting Information S1

Correspondence to:
E. J. D'Sa,
ejdsa@lsu.edu

Citation:
D'Sa, E. J., Joshi, I., & Liu, B. (2018). Galveston Bay and coastal ocean optical-geochemical response to Hurricane Harvey from VIIRS ocean color. *Geophysical Research Letters*, *45*, 10,579–10,589. https://doi.org/10.1029/2018GL079954

Received 9 AUG 2018
Accepted 27 SEP 2018
Accepted article online 1 OCT 2018
Published online 12 OCT 2018

Galveston Bay and Coastal Ocean Optical-Geochemical Response to Hurricane Harvey From VIIRS Ocean Color

Eurico J. D'Sa[1], Ishan Joshi[1], and Bingqing Liu[1]

[1]Department of Oceanography and Coastal Sciences, Louisiana State University and Agricultural and Mechanical College, Baton Rouge, LA, USA

Abstract Dissolved and particulate organic carbon, suspended particulate matter concentrations, and their optical proxies colored dissolved organic matter absorption and backscattering coefficients were studied in Galveston Bay, Texas, following the extreme flooding of Houston and surrounding areas due to Hurricane Harvey (25–29 August 2017) using field and ocean color observations. A three-step empirical-semianalytic algorithm for determination of colored dissolved organic matter absorption and backscattering coefficients revealed the dynamics of dissolved organic carbon and particle distribution from Visible and Infrared Imaging Radiometric Suite ocean color. Environmental drivers, especially floodwater discharge and winds, strongly influenced the spatiotemporal distribution of dissolved/particulate material in the bay and shelf waters following the hurricane passage. Over 10 days during/following the hurricane, ~25.2×10^6 kg C of total organic carbon and ~314.7×10^6 kg of suspended particulate matter were rapidly exported from Galveston Bay (representing ~0.65% and 0.27% of respective annual Mississippi River fluxes to the Gulf of Mexico), with potential for ecological impacts to shelf waters.

Plain Language Summary Hurricane Harvey (25–29 August 2017), after making landfall on the Texas coast, deposited unprecedented rainfall (>500 mm) that caused widespread flooding in the highly industrialized Houston Metropolitan and surrounding areas with potential for elevated levels of dissolved and particulate matter in the floodwaters discharging into Galveston Bay. We used a combination of field and satellite ocean color observations to examine the hurricane impact of Hurricane Harvey on the dissolved organic carbon and suspended particulate matter concentrations and their optical proxies in Galveston Bay and surrounding coastal ocean. Results of this study indicate that estimate of fluxes of material exported from Galveston Bay to the coastal waters over a 10-day period during/following Hurricane Harvey was similar to that exported by a large river.

1. Introduction

Hurricane Harvey, after making landfall on the Texas coast as a category 4 hurricane on 25 August 2017, meandered inland, stalled, and deposited unprecedented rainfall that caused widespread flooding in the highly industrialized Houston Metropolitan and surrounding areas (>500 mm with return period >2,000 years under current climate and ~100 years by century end; Emmanuel, 2017) with potential for adverse ecological impacts due to elevated levels of dissolved and particulate organic matter (DOC and POC) and suspended particulate matter (SPM) in the floodwaters discharging into Galveston Bay. Thus, ability to monitor DOC, POC, and SPM or their optical proxies, chromophoric dissolved organic matter (CDOM), and scattering properties could provide insights into the bay's water quality and its distribution and transport into the coastal ocean following episodic events such as Hurricane Harvey, one of the most destructive hurricanes on record. Although field observations have generally provided a good understanding of the bay's geochemical properties (S. Lee et al., 2011; Wen et al., 2008), these are spatiotemporally limited, especially during extreme weather events. Satellite ocean color with its synoptic and near daily coverage has provided critical insights on the ocean's optical and biogeochemical response following hurricanes (D'Sa et al., 2010; Farfan et al., 2014; Lin et al., 2003; Lohrenz et al., 2008) but have been limited in the optically complex estuaries due to poor performance of the standard ocean color algorithms.

Empirical ocean color algorithms developed for many estuarine and coastal waters use remote sensing reflectance $R_{rs}(\lambda)$ band ratios (e.g., green to red bands) to relate to optical or geochemical quantities such as CDOM, SPM, or phytoplankton chlorophyll (Del Castillo & Miller, 2008; D'Sa et al., 2006, 2007; D'Sa &

Miller, 2003; Joshi et al., 2017; Joshi & D'Sa, 2015; Le et al., 2013; Mannino et al., 2014; Tehrani et al., 2013) and are often optimized for a particular estuary or season based on the dominant constituents influencing the absorption properties. In contrast, semianalytic algorithms which relate satellite-derived $R_{rs}(\lambda)$ to inherent optical properties (e.g., absorption a_t and backscattering b_b) through relationships such as $R_{rs} \cong b_b/(a_t + b_b)$ provide a more generalized approach to retrieve the absorption and scattering properties of seawater (Z. Lee et al., 2002; Zhu et al., 2011). For instance, absorption a_t, a dominant source of variability in water leaving radiance, is composed of contributions by water itself (a_w), phytoplankton (a_{phy}), CDOM (a_g), and nonalgal particulate matter (NAP; detrital and mineralogical particles; a_{NAP}) and can be expressed as $a_t = a_w + a_{phy} + a_g + a_{NAP}$, for wavelengths across the light spectrum. Variations in these constituent absorption properties have been mainly used to retrieve a_{phy} or combined $a_g + a_{NAP}$ (a_{dg}), as spectral shapes of CDOM and NAP absorption are similar and difficult to disentangle (Z. Lee et al., 2002). While these semianalytic relationships have been mainly developed for oceanic and coastal waters, more recently, a semianalytic approach has been proposed for estuaries and optimized for the Visible and Infrared Imaging Radiometric Suite (VIIRS) sensor (Joshi & D'Sa, 2018).

In this study, we present results of two field sampling surveys in Galveston Bay conducted approximately 1 and 2 months following Hurricane Harvey as part of a NASA Rapid Response project to assess the hurricane impact on the bay's water quality and bio-optical state. Satellite estimates of CDOM (a_g412) and NAP ($a_{NAP}412$) absorption coefficients at 412 nm and backscattering coefficient ($b_{bp}532$) at 532 nm were obtained from VIIRS using a combination of a new empirical and an estuarine tuned semianalytic algorithm (Quasi-Analytical Algorithm for VIIRS [QAA-V]; Joshi & D'Sa, 2018); then, using a series of cloud-free imagery from before and after the hurricane, the environmental drivers on a_g412 and $b_{bp}532$ distribution were examined. Finally, in situ hydrodynamic data (tides, currents, and river discharge) and satellite estimates of SPM, DOC, and POC concentrations at the bay entrance were used to determine export fluxes of these constituents to the coastal ocean during and immediately following Hurricane Harvey.

2. Data and Methods

2.1. Study Site and Field Sampling

Galveston Bay, a wide and shallow estuary (~2-m average depth; 1,600-km^2 area) located along the upper coast of Texas (Figure 1a) is the seventh largest estuary in the continental United States. Major sources of freshwater to the estuary are the Trinity River (TR, ~50%), the San Jacinto River (SJR, ~30%), and local watersheds surrounding Galveston Bay (~20%; Guthrie et al., 2012; Lucena & Lee, 2017). The Houston Ship Channel is a deep (~14 m) and narrow channel connecting the bay to the northern Gulf of Mexico (GOM) through a narrow entrance, the Bolivar Roads Pass (Figure 1a). The bay region sampled in this study includes Trinity Bay (TB), Upper Galveston Bay (UGB), Lower Galveston Bay (LGB), and coastal stations near the bay entrance (Figures 1a and 3). Two field surveys were conducted on 29 September (survey1) and 29/30 October 2017 (survey2), respectively, following Hurricane Harvey. During both field surveys, surface water samples were collected along a transect from the riverine end-member of the TR to the head of the estuary (Figure 1a; orange circles). Sampling at additional sites was conducted in the UGB and East Bay during survey2 (white circles).

2.2. Optical and Geochemical Measurements

Surface water samples were filtered through 0.2-μm prerinsed Nuclepore filters on the same day and stored in acid-cleaned, precombusted amber bottles with Teflon-lined caps at 4 °C in the dark and processed within a week for CDOM spectral absorption on a dual-beam Perkin-Elmer Lambda 850 spectrophotometer; the absorption coefficient at 412 nm (a_g412) and spectral slope S between 275 and 295 nm were then determined (Joshi & D'Sa, 2015). Filtered samples were also processed for DOC on a Shimadzu total organic carbon analyzer (TOC-5000A) using a high-temperature combustion method (Benner & Strom, 1993; D'Sa et al., 2016). For determinations of light absorption by SPM, particles were collected onto 25-mm-diameter Whatman GF/F filter and stored in liquid nitrogen until measurement. Particulate (total and nonalgal) absorption were measured on a Perkin-Elmer Lambda 850 spectrophotometer fitted with a 15-cm-diameter integrating sphere (Naik & D'Sa, 2012). SPM concentrations were determined by filtration through dry preweighed Whatman GF/F filters (Joshi & D'Sa, 2018; Neukermans et al., 2012). An optical package with a Wetlabs ecotriplet and a Sea-Bird SBE conductivity-temperature-depth recorder was used to obtain measurements of chlorophyll and

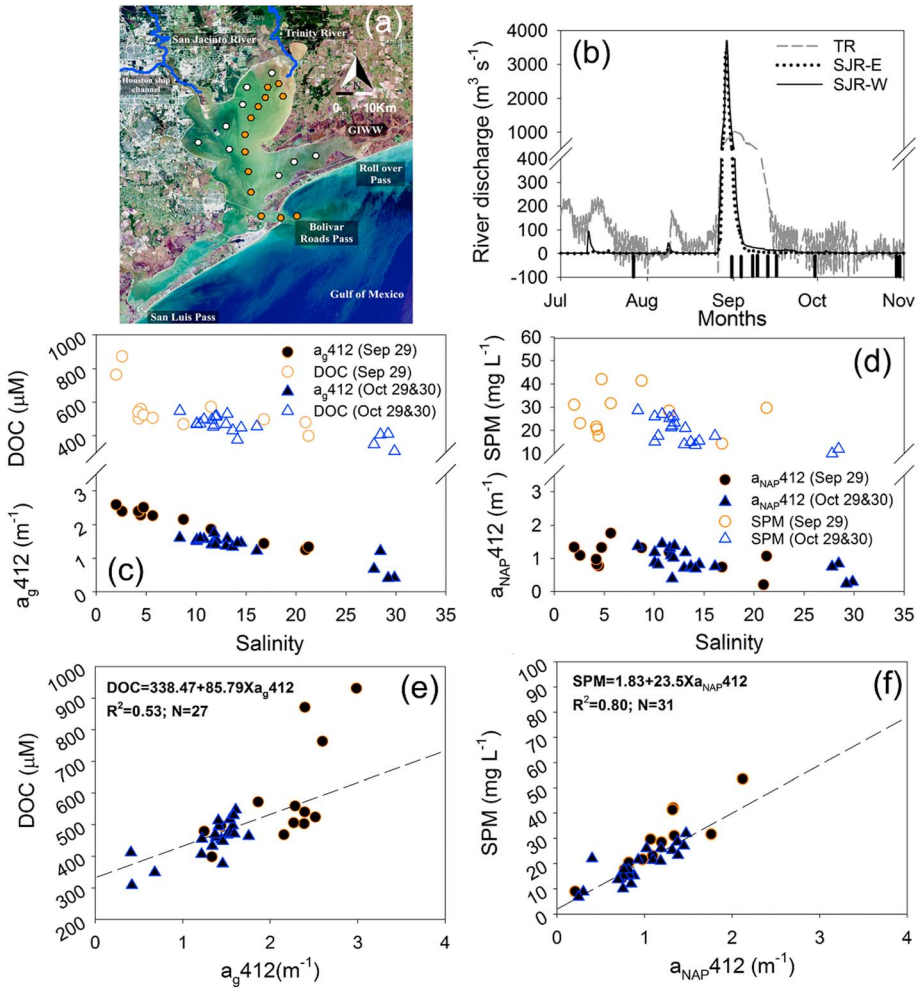

Figure 1. (a) Galveston Bay with sampling stations occupied on 29 September and 29 October 2017 (orange circles) and additional stations on 30 October 2017 (white circles). (b) Discharge from the TR and the SJR. Relationships (c) between salinity and a_g412 and between salinity and DOC, (d) between salinity and $a_{NAP}412$ and between salinity and SPM, (e) between a_g412 and DOC, and (f) between $a_{NAP}412$ and SPM. TR = Trinity River; SJR = San Jacinto River; DOC = dissolved organic carbon; SPM = suspended particulate matter.

CDOM fluorescence, backscattering, and salinity at the sampling stations (D'Sa et al., 2006; Joshi & D'Sa, 2018). Above-water measurements of water surface, sky, and reference plate radiances were collected using a GER 1500 512iHR spectroradiometer under clear-sky conditions to obtain above-water remote sensing reflectance (Rrs^{0+}, sr^{-1}) (Mobley, 1999; additional details in D'Sa & Miller, 2005; Joshi & D'Sa, 2018).

2.3. Ocean Color Satellite Data

VIIRS ocean color satellite data were obtained for clear-sky days from the NASA Ocean Biology Processing Group website for days before and after Hurricane Harvey including two field surveys on 30 September (+1 day as compared to field survey) and 29 and 30 October 2017. Satellite data were processed using the NASA SeaDAS 7.4 software and corrected for the atmosphere using the MUMM NIR scheme (Ruddick et al., 2006). Satellite imagery were further processed using the QAA-V to obtain estimates of $b_{bp}532$ and SPM (Joshi & D'Sa, 2018).

2.4. Hydrological, Meteorological, and Hydrodynamic Data

Discharge data were obtained from the U.S. Geological Survey gauge stations at Wallisville (~40 km from river mouth) for TR and the east and west fork stations for SJR (Figure 1b). Meteorological data (atmospheric pressure and winds) (Figure 2e) were obtained from a National Oceanic and Atmospheric Administration (NOAA)

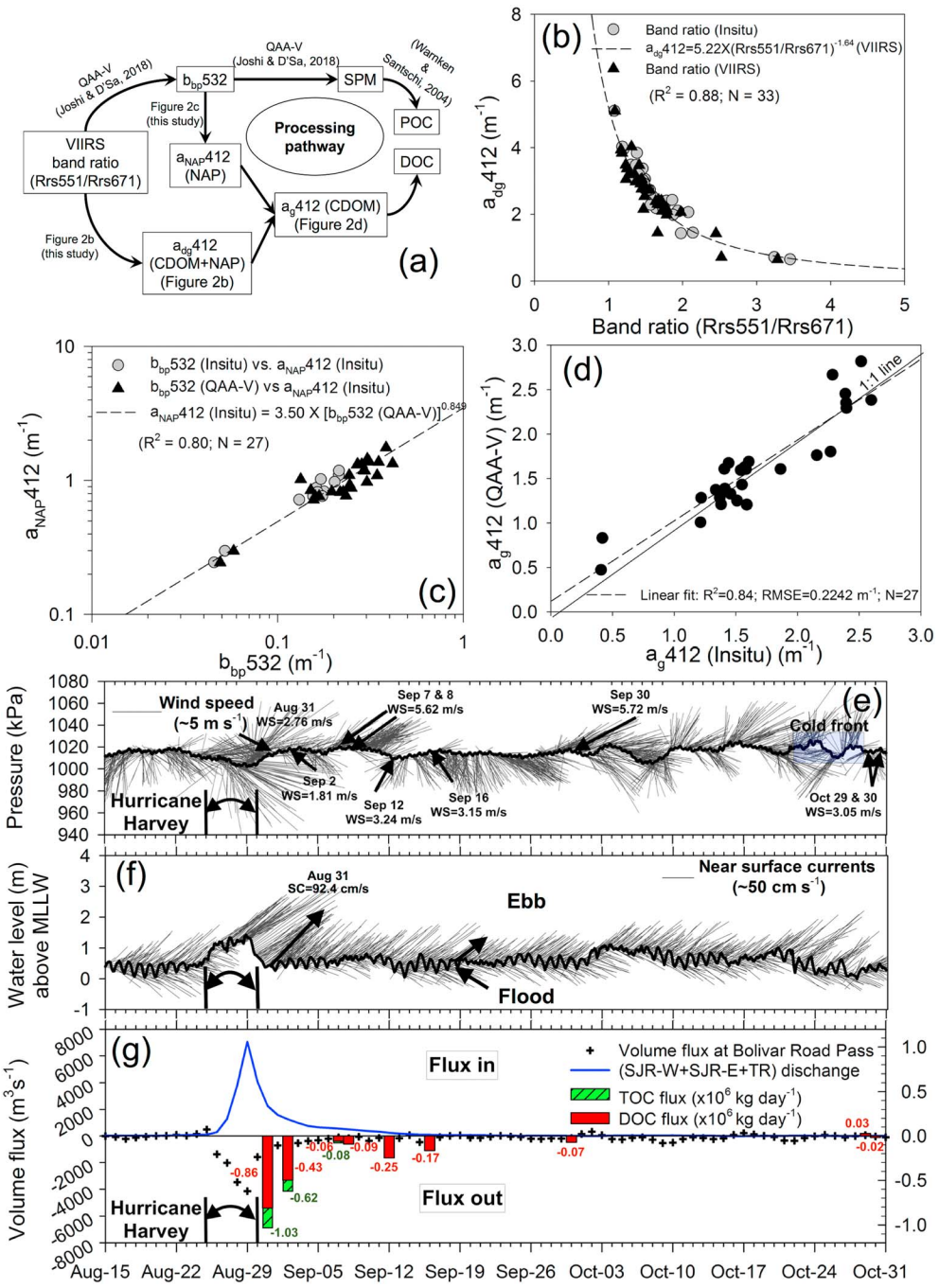

Figure 2. (a) Flowchart showing processing approach for obtaining VIIRS estimates of DOC and POC in Galveston Bay. Relationships between (b) band ratio $R_{rs}551/R_{rs}671$ (in situ and VIIRS derived) and in situ $a_{dg}412$ (a_g412 + $a_{NAP}412$), (c) VIIRS-derived (QAA-V) and in situ $b_{bp}532$ and in situ $a_{NAP}412$, and (d) validation matchups of in situ and VIIRS-derived a_g412. Time series of (e) atmospheric pressure and winds and (f) water level and surface currents at Galveston Bay entrance. (g) Discharge from TR + SJR; volume water, DOC and POC fluxes through the Galveston Bay entrance (+/− into/out of the bay). Black arrows (e) indicate the wind vectors corresponding to VIIRS satellite imagery. VIIRS = Visible and Infrared Imaging Radiometric Suite; DOC = dissolved organic carbon; POC = particulate organic carbon; QAA-V = Quasi-Analytical Algorithm for VIIRS; TR = Trinity River; SJR = San Jacinto River; SPM = suspended particulate matter; NAP = nonalgal particulate matter; CDOM = colored dissolved organic matter.

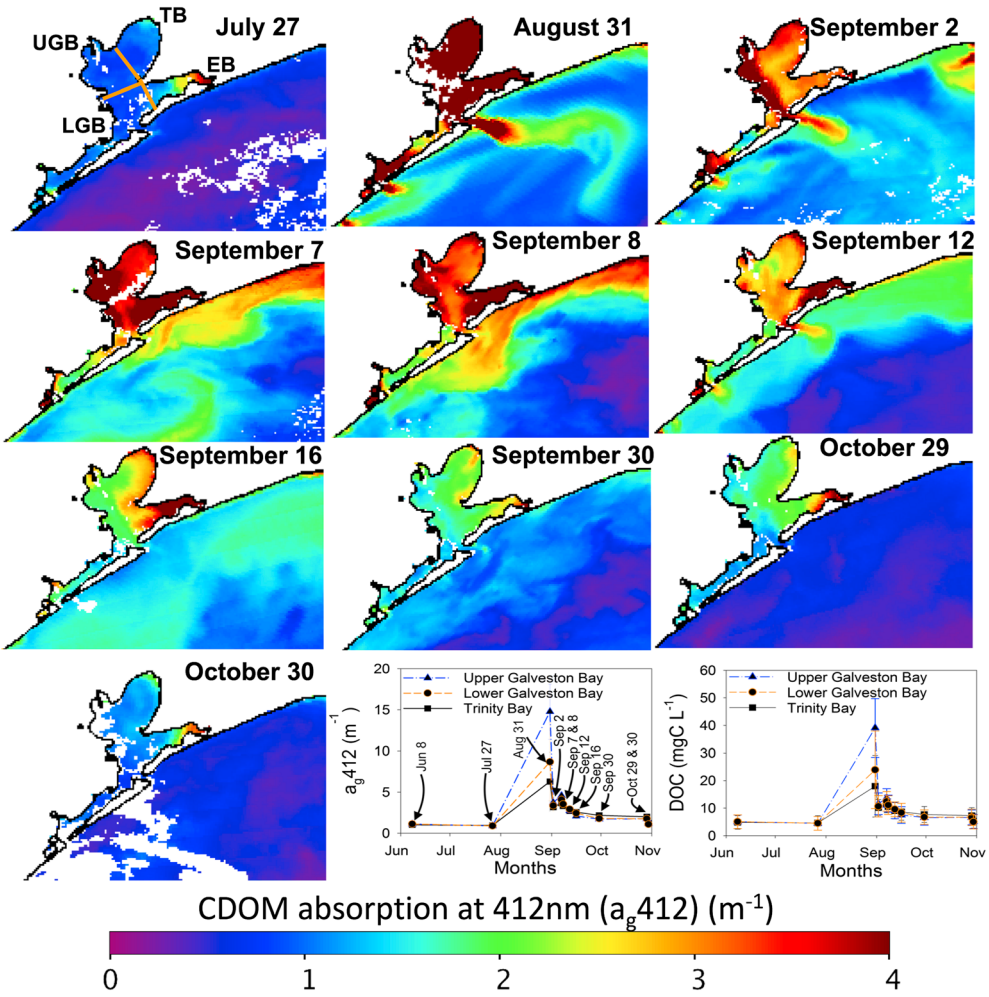

Figure 3. Sequence of VIIRS-derived a_g412 imagery of Galveston Bay and coast from before/after Hurricane Harvey. (bottom) mean satellite estimates of a_g412 and DOC concentrations in the three subbays. VIIRS = Visible and Infrared Imaging Radiometric Suite; DOC = dissolved organic carbon; CDOM = colored dissolved organic matter; TB = Trinity Bay; UGB = Upper Galveston Bay; LGB = Lower Galveston Bay; EB = East Bay.

station at Eagle Point, Galveston. Hydrodynamic data (tides and currents) were obtained from the NOAA tides and currents (ADCP) station located at the entrance of Galveston Bay. Mean lower low water (MLLW) which is the National Ocean Service's nautical chart data and mean sea level (MSL) values which are available at hourly intervals were downloaded from NOAA's website. A 40-hr low-pass filter was used to remove the tidal variation (range $<$ 0.5 m) from MSL. The difference between the local MSL and MLLW is the nontidal component or residual water level that is due to river flow and winds (Figure 2f). Near-surface currents (speed and direction) were normalized along the bay entrance with current vectors shown above the water level line being directed out of the bay (e.g., ebb tide) while current vectors located below the water level line are directed into the bay (e.g., flood tide).

2.5. Water Volume and Carbon Flux Calculations

The daily water volume flux (positive—inward; negative—outward; Figure 2g) through the Bolivar Roads Pass entrance was calculated by integrating the hourly flows across the bay entrance as follows:

$$\text{Water volume transport} = \text{current}\ (\text{m/s}) \times \text{Pass cross} - \text{sectional area}\ (\text{m}^2) \quad (1)$$

where the currents are directed inward (flood) or outward (ebb) of the bay (Figure 2f). The cross-sectional area was calculated as the residual water level (detided MSL − MLLW) × width of the channel. DOC flux

rates for days with cloud-free VIIRS satellite imagery were computed by multiplying the mean satellite-derived DOC concentration across the channel by the net volume of water transported through the pass (Joshi et al., 2017). DOC fluxes between 26 August and 4 September corresponding to high river discharge and water volume export (Figure 2g) were calculated by converting the daily water fluxes to daily DOC fluxes (based on a linear correlation between the two parameters) and then integrating the fluxes over the 10-day period (similarly, for SPM and POC). DOC fluxes over a 1-month period (26 August to 26 September 2017) were also estimated.

3. Results and Discussion

3.1. Hydrologic Conditions and Optical-Geochemical Properties in Galveston Bay

River discharge was typical for SJR and TR (~1.52 and ~40.93 m^3/s) for the month of August before Hurricane Harvey. However, for a short period during and after the hurricane passage, discharge peaked on 29 August for the eastern and western flanks of the SJR (3,367.70 and 3,707.30 m^3/s) and for TR (1,035.28 m^3/s) on 31 August. Discharge, however, dropped to low values for SJR by 4 September but remained elevated till mid-September for TR, likely due to flooding over a larger drainage basin, to controlled water-release from reservoirs and its passage through wetlands of the lower Trinity Basin (Figure 1b).

Although discharge from TR was typical for September (26.6 m^3/s), salinity in Galveston Bay was lower during survey1 (2.00–21.25) than during survey2 (10.06–27.81) and generally lower than reported for the bay for the season (Han et al., 2006). DOC concentrations ranged from 852.4 to 394.84 μM C during survey1 and from 468.14 to 308.50 μM C during survey2, showing a general decrease with increasing salinity along the transect (Figure 1c). a_g412 (the DOC optical proxy) ranged from 2.98 (near TR) to 1.24 m^{-1} (coastal station) during survey1 and 1.73 to 0.41 m^{-1} during survey 2, generally decreasing with increasing salinity (Figure 1c). Corresponding mean values of spectral slope S were 17.85 ± 0.34 μm^{-1} during survey1 and 20.11 ± 0.71 μm^{-1} during survey 2. High CDOM, low S, and high DOC during survey1 indicate strong terrestrial signature with little photodegradation of the dissolved organic matter pool compared to survey2. CDOM absorption has not been previously reported for the bay; however, mean values of a_g412 (2.13 ± 0.52 m^{-1}) during survey1 were relatively higher than previously reported for coastal and estuarine waters (D'Sa, 2008; Mannino et al., 2014; Tehrani et al., 2013). Overall, for the two surveys, DOC was significantly related to CDOM (Figure 1e) as follows:

$$DOC = 338.47 + 85.79 \times a_g412 \quad \left(R^2 = 0.53, N = 27\right) \tag{2}$$

Similar relationships between DOC and CDOM absorption have been reported in other coastal and estuarine waters (Joshi et al., 2017; Tehrani et al., 2013). SPM was higher and more variable during survey1 (27.94 ± 12.36; min = 8.92, max = 53.50 mg/L) than during survey2 (18.49 ± 6.39; min = 6.8, max = 28.67 mg/L); overall it showed a decreasing trend with increasing salinity (Figure 1d). Similarly, $a_{NAP}412$, was also greater and more variable during survey1 (1.13 ± 0.48; min = 0.21, max = 2.11 m^{-1}) than survey2 (0.90 ± 0.34; min = 0.24, max = 1.44 m^{-1}) and showed decreasing trends with increasing salinity (Figure 1d). $a_{NAP}412$ values were greater than those previously reported for coastal waters of the northern GOM (D'Sa et al., 2007; Naik et al., 2011) and appeared to be well correlated to SPM in these turbid estuarine waters (Figure 1f). Particle (NAP plus phytoplankton) backscattering $b_{bp}532$ was also found to be well correlated to SPM in coastal waters including Galveston Bay (R^2 = 0.89; equation (16), Joshi & D'Sa, 2018), with a relationship given by

$$SPM = 103.07 \times b_{bp}532 + 0.24 \tag{3}$$

Furthermore, a previously reported relationship between POC and SPM for Galveston Bay (Warnken & Santschi, 2004) was used to derive POC using the equation

$$POC^* = 725.60 \times SPM^{-0.701} \tag{4}$$

where POC* = POC/SPM. These relationships indicate a strong link between the optical and the geochemical properties. Furthermore, lower salinity and higher levels of DOC and SPM including their optical proxies

during survey1 compared to earlier reported measurements strongly indicate longer-term hurricane impact on the bay's geochemical properties.

3.2. VIIRS Estimates of CDOM/NAP Absorption and DOC/SPM/POC Concentrations

A comparison of in situ versus VIIRS-derived *Rrs* revealed a good agreement for the green and red bands, compared to blue (Joshi & D'Sa, 2018, Table 4). Thus, using a green to red band ratio, the combined CDOM+NAP ($a_{dg}412$), followed by individual $a_{NAP}412$ and a_g412 absorption coefficients, were obtained using the following steps (schematic, Figure 2a): (i) A *Rrs551/Rrs671* band ratio (VIIRS and in situ) was observed to be highly correlated to $a_{dg}412$ with a power law equation (Figure 2b) given by

$$a_{dg}412 = 5.22 \times \left(\frac{Rrs551}{Rrs671}\right)^{-1.64} \qquad \left(R^2 = 0.88; N = 33\right) \tag{5}$$

(ii) $b_{bp}532$ was derived from VIIRS using an estuarine tuned semianalytic algorithm (QAA-V; Joshi & D'Sa, 2018), (iii) a relationship between $b_{bp}532$ and $a_{NAP}412$ using both field and satellite observations (Figure 2c) was determined as

$$a_{NAP}412 = 3.50 \times \left(b_{bp}532_{QAA-V}\right)^{0.849} \qquad \left(R^2 = 0.80, N = 27\right). \tag{6}$$

This relationship was highly correlated and used to obtain estimates of $a_{NAP}412$ from VIIRS.

(iv) a_g412 was then determined from the equation

$$a_g412 = a_{dg}412 - a_{NAP}412 \tag{7}$$

VIIRS-derived a_g412 was found to be well correlated to in situ a_g412 (Figure 2d and supporting information Figure S1 show additional in situ validation of modeled/VIIRS-derived parameters). DOC was then determined from VIIRS imagery using equation (2), while SPM was determined from $b_{bp}532$ (QAA-V) using equation (3) (Joshi & D'Sa, 2018). Finally, POC was determined from SPM using equation (4).

3.3. Dissolved/Particulate Matter Distribution and Environmental Drivers

A series of cloud-free VIIRS imagery obtained before and after Hurricane Harvey were used to assess a_g412 and $b_{bp}532$ distributions (Figures 3 and 4), the optical proxies for DOC and SPM/POC, respectively. During this period, physical drivers such as river discharge, tides, and strong winds appear to have influenced the bay's optical-geochemical properties (Figures 2e–2g, 3, and 4). About 1 month before Hurricane Harvey impacted the Texas coast, mean VIIRS-derived surface a_g412 (0.89 m^{-1}) and $b_{bp}532$ (0.12 m^{-1}) within the bay (Figures 3 and 4 and Table S1) were comparable to those reported in coastal waters of northern GOM (D'Sa, 2008; D'Sa et al., 2007); corresponding estimates of DOC (4.52 mg C/L), POC (1.34 mg C/L), and SPM (12.55 mg/L) were generally typical for the summer (Hung et al., 2001). However, 2 days after the hurricane passage (31 August), estimates of a_g412 (6.29, 14.77, 8.67 m^{-1}) and $b_{bp}532$ (1.01, 1.84, 2.97 m^{-1}) increased to very high levels in TB, UGB, and LGB, respectively. Corresponding estimates of DOC (17.95, 39.06, and 23.88 mg C/L), POC (2.29, 2.64, and 2.77 mg C/L), and SPM (103.81, 190.52, and 220.51 mg/L; Figures 3 and 4 and Table S1) were some of the highest recorded, with estimates higher in UGB and LGB than TB, indicating stronger impact from SJR. Furthermore, a very coherent plume extending well offshore suggests the massive injection of DOC/POC/SPM-laden freshwater tens of kilometers (~60 km on 31 August) into the shelf. Similar plumes of high CDOM/DOC and suspended particulate material into the shelf waters were observed from all the other bays and estuaries along the Texas-Louisiana coast (Figures S2 and S3) suggesting that in aggregate, this event transported massive amount of terrestrial carbon and suspended sediments into the coastal ocean with potential for long-term ecological impacts. Concentrations decreased significantly by 2 September (Figures 3 and 4 and Table S1), but high levels along the western bay indicated that the Houston Ship Channel formed an efficient conduit for transporting floodwaters discharged mainly through SJR into the coastal ocean due to its low residence time under high discharge conditions (Rayson et al., 2016).

By 7 and 8 September, concentrations of DOC, POC, and SPM were still elevated in comparison to 2 September, likely due to a cold front (strong northeasterly winds) related resuspension (Figure 2e). Satellite imagery revealed the dissipation of the plume and the westward advection of coastal waters (driven by strong northeasterly winds) with high CDOM and low NAP absorption (Figures S2 and S3). The origin of

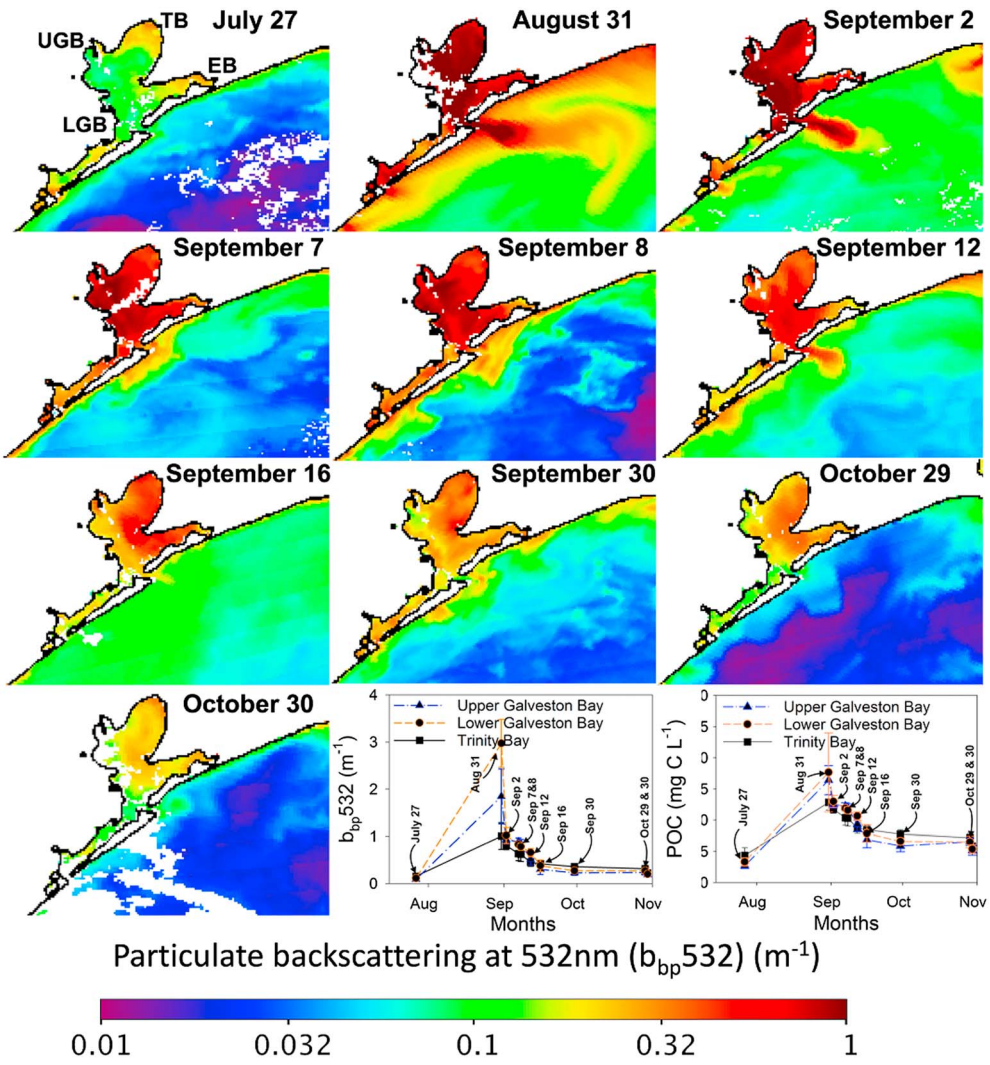

Figure 4. Sequence of VIIRS-derived $b_{bp}532$ imagery of Galveston Bay and coast from before/after Hurricane Harvey. (bottom) mean estimates of $b_{bp}532$ and POC concentrations in the three subbays. VIIRS = Visible and Infrared Imaging Radiometric Suite; POC = particulate organic carbon; TB = Trinity Bay; UGB = Upper Galveston Bay; LGB = Lower Galveston Bay; EB = East Bay.

these coastal waters appears to be Sabine Lake (a high refractory DOC environment; Bianchi et al., 1997) whose drainage basin was also strongly impacted by Hurricane Harvey. The advection of coastal waters into the bay (e.g., Rayson et al., 2015) with relatively high CDOM/low particle waters (Figures 3 and 4) could have changed the bay's geochemical properties. While bay waters continued flowing into the shelf through 12 September as a strong plume, spatial patterns of optical properties through October indicated that (i) CDOM was the dominant absorption constituent, with elevated values persisting longer in the surrounding coastal waters (Figures S2 and S3); (ii) by 16 September, with discharge from SJR to prehurricane levels, floodwaters appeared to be flushed out of the western bay (low CDOM/particle scattering) but were elevated in the eastern bay, likely due to elevated discharge from TR and wetlands runoff and longer residence times of TB and East Bay (Rayson et al., 2016); (iii) while the hurricane resulted in longer-term increases in DOC/POC/SPM, cold fronts appear to cause only short-term increases in these constituents; and (iv) the fraction of organic content of particles (POC/SPM) decreased considerably from ~10.7% in July to ~1.3% during the 10-day high river discharge period, subsequently increasing with time (Figure 4—bottom and Table S1) and generally consistent with earlier studies (e.g., Warnken & Santschi, 2004). In the shelf, DOC and SPM (Joshi & D'Sa, 2018) showed large along- and cross-shelf variability influenced by plume strength, coastal currents, and frontal passages.

3.4. Dissolved/Particulate Matter Fluxes to the Coastal Ocean

The combined discharge from SJR and TR into the bay peaked (7,058.02 m^3/s) on 28 August with dominant contribution from SJR (6,282.6 m^3/s). Simultaneously, the volume water flux out of the bay increased steadily to a peak of ~4,146.5 m^3/s on 28 August that coincided with a twofold increase in water level (1.11 ± 0.19 m above MLLW) and high outward surface currents (2.25 m/s) at the bay entrance (Figures 1b, 2f, and 2g) resulting in rapid flushing of floodwaters out of the bay and into offshore shelf waters as indicated by the imagery of 31 August (Figures 3 and 4). Overall, during and following the hurricane, the ebb tidal current (northeast) was generally much stronger than the flood tidal current (northwest; Figure 2f) due to the large volume of floodwaters in the bay. From a linear relationship observed between SPM and the river discharge (not shown) and assuming well-mixed waters under strong flows, SPM export from the bay (mainly terrestrial material associated with floodwaters from SJR basin) between 26 August and 4 September was estimated at 314.7×10^6 kg (peak export of 163.8×10^6 kg on 29 August 2017), representing ~0.27% of the annual Mississippi River suspended sediment loading to the northern GOM (Meade & Moody, 2010). Estimates of DOC and POC exported to the shelf was 0.86×10^6 and 0.20×10^6 kg C on 31 August and 0.43×10^6 and 0.19×10^6 kg C on 2 September, respectively. DOC flux reduced to ~0.11×10^6 and 0.02×10^6 kg C on 7/8 September due to wind-driven advection of coastal waters into the bay. DOC flux increased again on 12 September to 0.25×10^6 kg C. The integrated export of total organic flux (DOC plus POC) over a 10-day period between 26 August and 4 September was 25.22×10^6 kg C ($21.6 \times 10^6 + 3.57 \times 10^6$ kg C), representing ~0.63% of the total annual organic flux by the Mississippi River to the northern GOM (4.0×10^9 kg C; Bianchi et al., 2007). The peak DOC flux export of 9.43×10^6 kg C on 29 August 2017 was in the range of the daily flux export of the Mississippi River (~8.49×10^6 kg/day; Bianchi et al., 2004; Del Castillo & Miller, 2008) or that exported by all the major estuaries to the mid-Atlantic Bight over a 10-day period (Mannino et al., 2015). Over the next 20 days (to 26 September), the total DOC flux exported out of Galveston Bay was estimated at 1.87×10^6 kg C, likely a contribution from the TR discharge and its greater residence time in TB (Grayson et al., 2016).

4. Conclusions

In this study, we used a combination of field and satellite ocean color observations to examine the impact of Hurricane Harvey on the bio-optical and geochemical properties in Galveston Bay and surrounding coastal ocean. Field data indicated that even 1 month following the hurricane-related flooding of the Texas coast, lower salinity prevailed over much of the bay with elevated levels of DOC and SPM concentrations. CDOM absorption and backscattering coefficients, the optical proxies for DOC, POC, and SPM, were estimated and validated from the VIIRS ocean color data using a combination of a new empirical and an estuarine tuned semianalytical algorithm. An analysis of a series of cloud-free VIIRS imagery of CDOM absorption and backscattering revealed a highly dynamic response of the dissolved (DOC) and particulate matter (SPM/POC) constituents in different subregions of the bay. The differences in the river discharge patterns and residence times of freshwater in the bay, and meteorological events greatly influenced the transport and distribution of dissolved and particulate material in the bay and the coastal ocean. The massive initial pulse of discharge from SJR (equivalent to the low flow from the Mississippi River) and its rapid flow through the shipping channel into the coastal waters likely prevented its distribution in the bay. However, its transport with minimal transformation likely transferred massive amounts of material to the coastal waters with potential to strongly influence its water quality and ecosystem that warrants long-term monitoring of the impacted coastal region. This study also demonstrates the application of novel ocean color algorithms for the relatively new VIIRS satellite sensor to elucidate the impact of extreme flooding on the dissolved and particulate matter dynamics in the coastal ocean.

Acknowledgments
The authors thank NASA Ocean Color Biology Processing Group (OBGP) for providing access to VIIRS data and Bill Gibson from Coastal Studies Institute for providing logistic support for field operations. Field data and data sources used in this study are provided in the supporting information. This work was supported by a NASA Rapid Response Grant 80NSSC18K0177.

References

Benner, R., & Strom, M. (1993). A critical evaluation of the analytical blank associated with DOC measurements by high temperature catalytic oxidation. *Marine Chemistry*, *41*(1-3), 153–160. https://doi.org/10.1016/0304-4203(93)90113-3

Bianchi, T. S., Baskaran, M., DeLord, J., & Ravichandran, M. (1997). Carbon cycling in a shallow turbid estuary of southeast Texas: The use of plant pigment biomarkers and water quality parameters. *Estuaries*, *20*(2), 404–415. https://doi.org/10.2307/1352353

Bianchi, T. S., Filley, T., Dria, K., & Hatcher, P. G. (2004). Temporal variability of dissolved organic carbon in the lower Mississippi River. *Geochimica et Cosmochimica Acta*, *68*(5), 959–967. https://doi.org/10.1016/j.gca.2003.07.011

Bianchi, T. S., Wysocki, L. A., Stewart, M., Filley, T. R., & McKee, B. A. (2007). Temporal variability in terrestrially-derived sources of particulate organic carbon in the lower Mississippi River and its upper tributaries. *Geochimica et Cosmochimica Acta*, *71*(18), 4425–4437. https://doi.org/10.1016/j.gca.2007.07.011

Del Castillo, C., & Miller, R. L. (2008). On the use of ocean color remote sensing to measure the transport of dissolved organic carbon by the Mississippi River plume. *Remote Sensing of Environment*, *112*(3), 836–844. https://doi.org/10.1016/j.rse.2007.06.015

D'Sa, E., Overton, J. E. B., Lohrenz, S. E., Maiti, K., Turner, R. E., & Freeman, A. (2016). Changing dynamics of dissolved organic matter fluorescence in the northern Gulf of Mexico following the Deepwater Horizon oil spill. *Environmental Science and Technology*, *50*(10), 4940–4950. https://doi.org/10.1021/acs.est.5b04924

D'Sa, E. J. (2008). Colored dissolved organic matter in coastal waters influenced by the Atchafalaya River, USA: Effects of an algal bloom. *Journal of Applied Remote Sensing*, *2*(1), 023502. https://doi.org/10.1117/1.2838253

D'Sa, E. J., Korobkin, M., & Ko, D. S. (2010). Effects of Hurricane Ike on the Louisiana-Texas coast from satellite and model data. *Remote Sensing Letters*, *2*, 11–19.

D'Sa, E. J., & Miller, R. L. (2003). Bio-optical properties in waters influenced by the Mississippi River during low flow conditions. *Remote Sensing of Environment*, *84*(4), 538–549. https://doi.org/10.1016/S0034-4257(02)00163-3

D'Sa, E. J., & Miller, R. L. (2005). Bio-optical properties of coastal waters. In R. L. Miller, C. Del Castillo, & B. McKee (Eds.), Chapter 6*Remote sensing of coastal aquatic environments* (pp. 129–155). Dordrecht, Netherlands: Springer.

D'Sa, E. J., Miller, R. L., & Del Castillo, C. (2006). Bio-optical properties and ocean color algorithms for coastal waters influenced by the Mississippi River during a cold front. *Applied Optics*, *45*(28), 7410–7428. https://doi.org/10.1364/AO.45.007410

D'Sa, E. J., Miller, R. L., & McKee, B. A. (2007). Suspended particulate matter dynamics in coastal waters from ocean color: Application to the northern Gulf of Mexico. *Geophysical Research Letters*, *34*, L23611. https://doi.org/10.1029/2007GL031192

Emmanuel, K. (2017). Assessing the present and future probability of Hurricane Harvey's rainfall. *Proceedings National Academy of Sciences USA*, *114*(48), 12,681–12,684. https://doi.org/10.1073/pnas.1716222114

Farfan, L. M., D'Sa, E. J., Liu, K., & Rivera-Monroy, V. H. (2014). Tropical cyclone impacts on coastal regions: The case of the Yucatan and the Baha California peninsulas, Mexico. *Estuaries and Coasts*, *37*(6), 1388–1402. https://doi.org/10.1007/s12237-014-9797-2

Guthrie, C. G., Matsumoto, J., & Solis, R. S. (2012). *Analysis of the influence of water plan strategies on inflows and salinity in Galveston Bay* (p. 71). Austin, Texas: *United States Army Corps of Engineers,* Texas Water Development Board.

Han, S., Gill, G. A., Lehman, R. D., & Choe, K.-Y. (2006). Complexation of mercury by dissolved organic matter in surface waters of Galveston Bay, Texas. *Marine Chemistry*, *98*(2-4), 156–166. https://doi.org/10.1016/j.marchem.2005.07.004

Hung, C.-C., Tang, D., Warnken, K. W., & Santschi, P. H. (2001). Distributions of carbohydrates, including uronic acids, in estuarine waters of Galveston Bay. *Marine Chemistry*, *73*(3-4), 305–318. https://doi.org/10.1016/S0304-4203(00)00114-6

Joshi, I., & D'Sa, E. J. (2015). Seasonal variation of colored dissolved organic matter in Barataria Bay, Louisiana, using combined Landsat and field data. *Remote Sensing*, *7*(9), 12,478–12,502. https://doi.org/10.3390/rs70912478

Joshi, I. D., & D'Sa, E. J. (2018). An estuarine tuned Quasi-Analytical Algorithm for VIIRS (QAA-V): Assessment and application to satellite estimates of SPM in Galveston Bay following Hurricane Harvey. *Biogeosciences*, *15*(13), 4065–4086. https://doi.org/10.5194/bg-15-4065-2018

Joshi, I. D., D'Sa, E. J., Osburn, C. L., Bianchi, T. S., Ko, D. S., Oviedo-Vargas, D., et al. (2017). Assessing chromophoric dissolved organic matter (CDOM) distribution, stocks, and fluxes in Apalachicola Bay using combined field, VIIRS ocean color, and model observations. *Remote Sensing of Environment*, *191*, 359–372. https://doi.org/10.1016/j.rse.2017.01.039

Le, C., Hu, C., English, D., Cannizzaro, J., & Kovach, C. (2013). Climate-driven chlorophyll-a changes in a turbid estuary: Observations from satellites and implications for management. *Remote Sensing of Environment*, *130*, 11–24. https://doi.org/10.1016/j.rse.2012.11.011

Lee, S., Han, S., & Gill, G. A. (2011). Estuarine mixing behavior of colloidal organic carbon and colloidal mercury in Galveston Bay, Texas. *Journal of Environmental Monitoring*, *13*(6), 1703–1708. https://doi.org/10.1039/c0em00666a

Lee, Z., Carder, K. L., & Arnone, R. A. (2002). Deriving inherent optical properties from water color: A multiband quasi-analytical algorithm for optically deep waters. *Applied Optics*, *41*(27), 5755–5772. https://doi.org/10.1364/AO.41.005755

Lin, I., Liu, W. T., Wu, C.-C., Wong, G. T. F., Hu, C., Chen, Z., et al. (2003). New evidence for enhanced ocean primary production triggered by tropical cyclone. *Geophysical Research Letters*, *30*(13), 1718. https://doi.org/10.1029/2003GL017141

Lohrenz, S. E., Cai, W.-J., Chen, X., & Tuel, M. (2008). Satellite assessment of bio-optical properties of northern Gulf of Mexico coastal waters following Hurricanes Katrina and Rita. *Sensors*, *8*(7), 4135–4150. https://doi.org/10.3390/s8074135

Lucena, Z., & Lee, M. T. (2017). Characterization of streamflow, suspended sediment, and nutrients entering Galveston Bay from the Trinity River, Texas, May 2014–December 2015, Reston, VA, *USGS Numbered Series*, vii, 37 p.

Mannino, A., Novak, M. G., Hooker, S. B., Hyde, K., & Aurin, D. (2014). Algorithm development and validation of CDOM properties for estuarine and continental shelf waters along the northeastern U.S. coast. *Remote Sensing of Environment*, *152*, 576–602. https://doi.org/10.1016/j.rse.2014.06.027

Mannino, A., Signorini, S. R., Novak, M. G., Wilkin, J., Friedrichs, M. A. M., & Najjar, R. G. (2015). Dissolved organic carbon fluxes in the Middle Atlantic Bight: An integrated approach based on satellite data and ocean model products. *Journal of Geophysical Research: Biogeosciences*, *121*, 312–336. https://doi.org/10.1002/2015JG003031

Meade, R. H., & Moody, J. A. (2010). Causes for the decline of suspended-sediment discharge in the Mississippi River system, 1940–2007. *Hydrological Processes*, *24*, 35–49.

Mobley, C. D. (1999). Estimation of the remote-sensing reflectance from above-surface measurements. *Applied Optics*, *38*(36), 7442–7455. https://doi.org/10.1364/AO.38.007442

Naik, P., & D'Sa, E. J. (2012). Phytoplankton light absorption of cultures and natural samples: Comparisons using two spectrophotometers. *Optics Express*, *20*(5), 4871–4886. https://doi.org/10.1364/OE.20.004871

Naik, P., D'Sa, E. J., Grippo, M., Condrey, R., & Fleeger, J. (2011). Absorption properties of shoal-dominated waters in the Atchafalaya shelf, Louisiana, USA. *International Journal of Remote Sensing*, *32*(15), 4383–4406. https://doi.org/10.1080/01431161.2010.486807

Neukermans, G., Ruddick, K. G., & Park, Y. (2012). Optimization and quality control of suspended particulate matter concentration measurement using turbidity measurements. *Limnology and Oceanography: Methods*, *10*, 1011–1023.

Rayson, M. D., Gross, E. S., & Fringer, O. B. (2015). Modeling the tidal and sub-tidal hydrodynamics in a shallow, micro-tidal estuary. *Ocean Modelling*, *89*, 29–44. https://doi.org/10.1016/j.ocemod.2015.02.002

Rayson, M. D., Gross, E. S., Hetland, R. D., & Fringer, O. B. (2016). Time scales in Galveston Bay: An unsteady estuary. *Journal of Geophysical Research: Oceans*, *121*, 2268–2285. https://doi.org/10.1002/2015JC011181

Ruddick, K. G., De Cauwer, V., Park, Y.-J., & Moore, G. (2006). Seaborne measurements of near infrared water-leaving reflectance: The similarity spectrum for turbid waters. *Limnology and Oceanography*, *51*(2), 1167–1179. https://doi.org/10.4319/lo.2006.51.2.1167

Tehrani, N. C., D'Sa, E. J., Osburn, C. L., Bianchi, T. S., & Schaeffer, B. A. (2013). Chromophoric dissolved organic matter and dissolved organic carbon from Sea-Viewing Wide Field-of-View Sensor (SeaWiFS), Moderate Resolution Imaging Spectroradiometer (MODIS) and MERIS sensors: Case study for the northern Gulf of Mexico. *Remote Sensing*, *5*(3), 1439–1464. https://doi.org/10.3390/rs5031439

Warnken, K. W., & Santschi, P. H. (2004). Biogeochemical behavior of organic carbon in the Trinity River downstream of a large reservoir lake in Texas, USA. *The Science of the Total Environment*, *329*(1-3), 131–144. https://doi.org/10.1016/j.scitotenv.2004.02.017

Wen, L.-S., Warnken, K. W., & Santschi, P. H. (2008). The role of organic carbon, iron, and aluminium oxyhydroxides as trace metal carriers: Comparison between the Trinity River and the Trinity River estuary (Galveston Bay, Texas). *Marine Chemistry*, *112*(1-2), 20–37. https://doi.org/10.1016/j.marchem.2008.06.003

Zhu, W., Yu, Q., Tian, Y. Q., Chen, R. F., & Gardner, G. B. (2011). Estimation of chromophoric dissolved organic matter in the Mississippi and Atchafalaya river plume regions using above-surface hyperspectral remote sensing. *Journal of Geophysical Research*, *116*, C02011. https://doi.org/10.1029/2010JC006523